Brain structure-function coupling – relationship with language lateralisation

Ieva Andrulyte[1]*, Laure Zago[2], Gael Jobard[2], Herve Lemaitre[2], Peter N Taylor[3], Francois Rheault[4,5], Marc Joliot[2], Laurent Petit[2,5], Simon S Keller[1]

1 Department of Pharmacology and Therapeutics, Institute of Systems, Molecular and Integrative Biology, University of Liverpool, Liverpool, UK
2 Universite de Bordeaux, CNRS, CEA, IMN, UMR 5293, GIN, F-33000 Bordeaux, France;
3 Interdisciplinary Computing and Complex BioSystems Group, School of Computing Science, Newcastle University, UK
4 Université de Sherbrooke, Department of Computer Science, Sherbrooke, Québec, Canada
5 IRP OpTeam, CNRS Biologie, France - Université de Sherbrooke, Canada

***Corresponding author:**

Ieva Andrulyte

The BRAIN Lab, William Henry Duncan Building, 6 West Derby Street

Liverpool, L7 8TX

Email: andrulyte.is@gmail.com

Authors' OrchIDs:

IA 0000-0002-8691-4078, LZ 0000-0001-8235-2154, GJ 0000-0003-4536-0643, HL 0000-0002-5952-076X, PNT - 0000-0003-2144-9838, FMR 0000-0002-0097-8004, MJ - 0000-0001-7792-308X, LP 0000-0003-2499-5367, SSK 0000-0001-5247-9795

Running header: Structural function coupling and language lateralisation

Keywords: language lateralisation, diffusion MRI, rsfMRI, structure-function coupling, anterior insula, precentral sulcus, middle temporal gyrus

Abstract

Language is one of the most extensively studied lateralised cognitive functions in the human brain, predominantly relying on the left hemisphere in most individuals. However, the mechanisms by which a stable white matter architecture underpins individual language functions remain unclear. Previous studies have employed structural connectivity (SC) and functional connectivity (FC) coupling for individual fingerprinting and task decoding, suggesting that variability in brain entropy may serve as a distinguishing characteristic for language lateralisation. We examined a large cohort of healthy adults (n = 285) to investigate SC-FC coupling and identify markers distinguishing different language laterality groups. Functional connectivity was measured using resting-state fMRI (rsfMRI) time-series data, while structural connectivity was determined via probabilistic fibre tractography. SC-FC coupling was investigated using the SENSAAS language atlas and defined as the Pearson correlation between non-zero elements of regional structural and functional connectivity profiles. Group differences were assessed using the PALM toolbox in FSL. Our findings revealed that increased SC-FC coupling in the left precentral sulcus was associated with typical language lateralisation, while increased coupling in the right middle temporal gyrus and left anterior insula was observed in individuals with atypical language lateralisation ($pFDR < 0.05$). Non-lateralised individuals exhibited increased coupling in the left anterior insula compared to lateralised ($pFDR<0.05$). SC-FC coupling offers a promising framework to uncover functional and anatomical differences among individuals with varying language lateralisation. This regional specificity indicates that typical, atypical, and non-lateralised profiles rely on different structural-functional alignments, likely reflecting the recruitment of alternative pathways for language processing.

Introduction

Hemispheric language dominance refers to the brain's interhemispheric asymmetry in language function, with around 90% of healthy individuals relying primarily on the left hemisphere, while the remaining 10% exhibit atypical patterns, characterised by bilateral involvement or primary reliance on the right hemisphere (Andrulyte et al., 2024; Mazoyer et al., 2014). The study of language lateralisation has begun to adopt a connectomics framework (Andrulyte, Zago, et al., 2025; Labache et al., 2020), which conceptualises the brain as an interconnected network of structural and functional connections supporting communication, information processing, and cognitive integration (Hagmann et al., 2008). This framework encompasses structural connectivity (SC)—the anatomical wiring reconstructed through diffusion MRI and tractography (Basser et al., 1994; Maier-Hein et al., 2017; Turner et al., 1990)—and functional connectivity (FC)—the temporal synchronisation of neural activity between brain regions, measured via resting-state fMRI (rsfMRI) (Biswal et al., 1995). SC captures stable anatomical pathways, while FC reflects dynamic neural interactions that support cognitive processing and neural communication (Avena-Koenigsberger et al., 2018; Betzel, 2020; Sotiropoulos & Zalesky, 2019; Tao et al., 2015).

Advances in rsfMRI and diffusion MRI (dMRI) analysis methods have enabled network-based approaches for the investigation of the neural basis of language lateralisation. In healthy individuals, rsfMRI studies have found that atypical lateralisation is associated with greater interhemispheric connectivity (Labache et al., 2020) and weaker intra-hemispheric integration (Ibrahim et al., 2015). dMRI analyses further support these findings, showing increased fractional anisotropy (FA) in temporal regions bilaterally (Andrulyte et al., 2024; Andrulyte, Zago, et al., 2025) and higher nodal degree in the posterior middle temporal gyrus and posterior cingulate cortex in atypically lateralised people (Zahnert et al., 2023).

While rsfMRI and dMRI have independently contributed to our understanding of the connectome, their integration offers a more comprehensive framework for studying language lateralisation. SC-FC coupling—the relationship between the brain's structural architecture and functional activity—provides valuable insights into how neural circuits support cognitive processes (Skudlarski et al., 2008; Suárez et al., 2020). Hebb's principle, "neurons that fire together wire together," highlights that repeated co-activation of neurons strengthens synaptic connections, shaping structural networks that optimise neural processing (Hebb, 1949; Straathof et al., 2019). Although structural connectivity explains 50-60% of the variance in functional connectivity, deviations between the two (decoupling) are particularly prominent in higher-order brain regions such

as the default mode network, which supports integrative cognitive functions (Baum et al., 2020; Preti & Van De Ville, 2019; Sarwar et al., 2021). This hierarchical organisation reflects an evolutionary specialisation: tightly coupled unimodal regions support efficient sensory processing, while more flexible coupling in transmodal regions supports integrative and adaptive functions (Huntenburg et al., 2017; Margulies et al., 2016; Yeo et al., 2016).

Coupling between structural and functional networks is thought to underpin individual differences in cognitive flexibility and specialisation (Medaglia et al., 2017). For example, weaker coupling in transmodal regions has been linked to cognitive flexibility, promoting regional specialisation, which allows the brain to support unique behavioural repertoires (Preti & Van De Ville, 2019). The critical brain hypothesis, which suggests the brain operates near a balance of order and chaos to optimise adaptability, aligns with these principles (Shi et al., 2021). While originally grounded in electroencephalography (EEG) studies, it may extend to structure-function coupling, where maintaining such a balance could support efficient information processing. Disruptions to this balance, observed in conditions such as epilepsy and schizophrenia, impair cognition by destabilising the relationship between structural and functional connectivity (Fornito & Bullmore, 2015; Wu et al., 2020; Z. Zhang et al., 2011).

Although coupling between structural and functional networks has proven useful in profiling cognitive traits, its application to language lateralisation has been limited but promising. Effective connectome analyses, which infer causal relationships between structural pathways and functional interactions, have revealed distinct language-related networks that connect sensory and self-referential systems with syntactic and motor planning regions, highlighting the structural-functional basis of language processes (Rolls et al., 2022). One study, focusing specifically on language lateralisation, employed diffusion map embedding to derive individual functional connectomes. It found that left-lateralised individuals exhibit increased resting-state connectivity in key regions such as the left inferior frontal gyrus, left inferior parietal lobule, and left middle temporal gyrus (Langs et al., 2016). These studies highlight the promise of integrating rsfMRI and dMRI for understanding language lateralisation, yet no research to date has explicitly examined SC-FC coupling as a potential marker for language dominance.

This study aims to bridge existing gaps by investigating the relationship between connectivity strength in diffusion MRI and rsfMRI modalities and their coupling in relation to language lateralisation. Specifically, we have two key objectives: (1) to examine rsfMRI and diffusion MRI FA connectivity strength at the level of individual nodes to identify associations with language lateralisation, and (2) to assess macroscale SC-FC

coupling strength and its relationship with functional language lateralisation. To achieve this, we leverage the BIL&GIN dataset, which provides well-characterised classifications of individuals with typical and atypical language lateralisation (Mazoyer et al., 2016). By analysing structure-function coupling in these groups, this study aimed to evaluate its potential as a marker for language dominance. We hypothesise that distinct coupling patterns will emerge across groups, with left-lateralised individuals showing increased coupling in classical language areas, such as the inferior frontal gyrus and middle temporal gyrus in the dominant hemisphere, and atypically lateralised individuals exhibiting reduced coupling.

Methods

Data acquisition

Structural and functional neuroimaging data were sourced from the BIL&GIN database, specifically designed to investigate the structural and functional neural correlates of brain lateralisation (Mazoyer et al., 2016). This study utilised data from 285 healthy individuals (aged 18-57 years; 48% female), including individual measures derived from diffusion MRI and resting-state functional MRI (rsfMRI) time-series.

Imaging data were acquired using a Philips Achieva 3-Tesla MRI scanner. The structural MRI protocol included a localiser scan and a high-resolution 3D T1-weighted sequence. The T1-weighted imaging parameters were as follows: repetition time (TR) = 20 ms, echo time (TE) = 4.6 ms, flip angle = 10° , inversion time = 800 ms, turbo field echo factor = 65, SENSE factor = 2, field of view (FOV) = 256 × 256 × 180 mm^3, and isotropic voxel size = 1 mm^3. Functional data were acquired using T2*-weighted echo-planar imaging (EPI) with TR = 2 s, TE = 35 ms, flip angle = 80° , and 31 axial slices, with an isotropic voxel size of 3.75 × 3.75 × 3.75 mm^3. The FOV was consistent with the T2*-FFE acquisition. Functional imaging for a sentence production task (Mazoyer et al., 2016) included three runs, each comprising 192 T2*-weighted volumes. For rsfMRI, participants underwent an 8-minute scan with instructions to keep their eyes closed, stay relaxed, minimise movement, remain awake, and let thoughts flow freely.

Diffusion-weighted imaging (DWI) employed a single-shot spin-echo EPI sequence. The protocol included a b0 image (b = 0 s/mm^2) and 21 non-collinear diffusion gradient directions (b = 1000 s/mm^2), each acquired twice with reversed gradient polarities. Gradient directions were evenly distributed across a half-sphere, with complementary directions on the opposing half-sphere. To enhance signal-to-noise ratio, the acquisition was repeated, resulting in a total scan time of 15 minutes and 30 seconds. Seventy axial slices were collected, aligned parallel to the anterior commissure-posterior commissure

(AC-PC) plane, spanning from the cerebellum base to the vertex. The imaging parameters included TR = 8500 ms, TE = 81 ms, flip angle = 90° , SENSE reduction factor = 2.5, acquisition matrix = 112 × 112, and an isotropic voxel size of 2 × 2 × 2 mm^3.

Language lateralisation

To assess language laterality, we utilised the sentence production task from the BIL&GIN dataset (Mazoyer et al., 2016) during a task-based fMRI session, employing a word-list production contrast. For the sentence production task, participants were presented with stimuli derived from the classic French comic strip series Le Petit Nicolas. After observing a "Le petit Nicolas" line drawing, participants were instructed to covertly generate a sentence structured as follows: a subject and complement, followed by a verb describing the action, and concluding with an additional complement specifying place or manner. In contrast, during the reference word production task, scrambled drawings served as stimuli, and participants were instructed to covertly generate a list of the months of the year. Further details on these tasks can be found in Mazoyer et al. (2016).

Language production laterality indices (LIs) were computed using the LI toolbox (Wilke & Schmithorst, 2006). The analysis was conducted within grey and white matter anatomical template masks, excluding the cerebellum, to maintain consistency with fMRI data normalisation protocols. The LI toolbox generated 10,000 potential LI combinations, and the central 50% were retained to mitigate the influence of statistical outliers. Final HFLI values, ranging from −100 (indicating exclusive right-hemisphere activation) to +100 (exclusive left-hemisphere activation), were calculated by weighting the central 50% of LIs based on their corresponding thresholds. To categorise individuals as lateralised, we used an LI threshold of 20, classifying individuals with $|LI| > 20$ as lateralised and those with $|LI| \leq 20$ as non-lateralised (i.e. bilateral).

To distinguish between atypically and typically lateralised individuals, we applied a threshold, defining individuals with $LI > 20$ as "typically" lateralised and those with lower values as "atypically" lateralised (Chang et al., 2017). Unlike prior studies (Andrulyte, Zago, et al., 2025), where atypical individuals were divided into two subgroups (e.g., right-lateralised and non-lateralised), we combined these groups into a single atypical category here to enhance interpretability and statistical power. In this study, we examined the effects of lateralisation versus bilaterality and typical versus atypical lateralisation separately, aiming to identify distinct components contributing to these differences.

Functional MRI data processing

Both resting-state and task-related fMRI data were processed using the global linear modelling software Statistical Parametric Mapping (SPM5; www.fil.ion.ucl.ac.uk/spm/) alongside customised MATLAB routines. Functional data from the three slow fMRI runs (gradient echo planar imaging, repetition time [TR] = 2.0 s, voxel size = 3.75 × 3.75 × 3.75 mm^3; acquired on a 3T Philips Intera Achieva scanner) underwent slice-timing and motion correction. Movement artefacts were mitigated by regressing the six motion parameters (three translations and three rotations) from each voxel's T2*-EPI time series. The corrected T2*-EPI scans were rigidly co-registered to the participants' structural T2*-FFE images.

The T1-weighted (T1w) volumes were segmented into grey matter, white matter, and cerebrospinal fluid. Spatial normalisation was performed by integrating the transformation matrix from T2*-FFE to T1w images with the stereotaxic normalisation matrix derived from T1w images. This process enabled the warping of T2*-EPI scans into standard stereotaxic space (2 × 2 × 2 mm^3 voxel resolution) using a single trilinear interpolation. Finally, voxel time series were high-pass filtered with a 159-second cut-off to remove low-frequency drifts (Joliot et al., 2016).

Resting-state fMRI connectivity mapping

Functional connectivity was assessed by extracting resting-state fMRI time-series data from 64 supramodal sentence-related regions defined by the SENSAAS language atlas, comprising 32 left-lateralised ROIs and their homotopic counterparts in the right hemisphere (Labache et al., 2019) (Figure 1). Pearson correlation coefficients were then computed between these regions to generate a correlation matrix capturing interregional functional connectivity (Sarwar et al., 2021). To improve clarity and facilitate interpretation, negative correlations within each connectivity matrix were replaced with zero values (Luppi & Stamatakis, 2021).

Diffusion MRI data processing

Probabilistic tractography was performed using TractoFlow, an automated diffusion MRI processing pipeline. TractoFlow integrates two tracking algorithms—classical local tracking and Particle Filter Tracking (PFT) (Girard et al., 2014) – to generate whole-brain tractograms. Diffusion MRI data were acquired using a spin-echo echo-planar imaging sequence with a b0 map and 84 diffusion-weighted images (b = 1000 s/mm^2), which were averaged in sets of four to yield 21 unique non-collinear diffusion directions. The diffusion signal was modelled using spherical harmonics of order 6 (Descoteaux et al., 2009). Whole-brain seeding was conducted, with PFT employing 10 seeds per voxel and local

tracking using 5 seeds per voxel. The default TractoFlow parameters were used, including a step size of 0.5 mm and a maximum angular deviation of 20° between steps.

To ensure anatomical consistency, tractograms were normalised to MNI space using ANTs (Avants et al., 2009). The transformation parameters, including both affine and nonlinear components derived from the registration of T1-weighted images to the MNI152 2009 standard-space template (1 mm isotropic resolution; Legarreta et al., 2021), were applied to warp the whole-brain tractograms.

To refine the tractograms, false-positive tracts were removed using the ExTractorFlow pipeline, which applies rule-based filtering grounded in neuroanatomical organisational principles. The method classifies streamlines as anatomically implausible if they violate known white matter architecture, such as forming 360° loops, terminating along the ventricles, fragmenting within deep white matter structures, or being shorter than 20 mm. This ensures that only streamlines following known pathways—association, commissural, and projection fibres—are retained. Further methodological details can be found in Petit et al. (2023). Thus, this approach enhances reproducibility and precision compared to conventional diffusion MRI techniques, enabling more accurate identification of anatomically plausible connections through region-of-interest filtering.

Diffusion MRI connectivity mapping

Structural connectivity was assessed using the same AICHA parcellation as in the rsfMRI analysis (Joliot et al., 2015), defining 384 brain regions (192 per hemisphere). Whole-brain tractograms were segmented into connectivity matrices using Scilpy toolbox (https://github.com/scilus/scilpy), where nodes corresponded to the parcellated brain regions and edges represented the white matter tracts linking them. Edges were weighted by fractional anisotropy (FA) values, which were chosen over streamline count due to its reduced susceptibility to biases inherent in probabilistic tractography (F. Zhang et al., 2022). While FA is sensitive to crossing fibres and other microstructural complexities (Jeurissen et al., 2013; Tournier et al., 2011), it remains widely used for structural network analyses (Lebel et al., 2019) and is a primary metric of interest in investigations of language lateralisation (Andrulyte, Demirkan, et al., 2025). The 384 × 384 connectivity matrices were downsampled to 64 × 64 by extracting 32 left-lateralised supramodal sentence-processing regions and their homotopic counterparts, as defined by the SENSAAS language atlas (Labache et al., 2019) (Figure 1).

Connectivity strengths for structural and functional connectivity and group comparisons

We calculated the average connectivity for each node in the SENSAAS atlas (Labache et al., 2019) in each subject using connectivity matrices derived separately from FA-based structural connectivity and rsfMRI functional connectivity. For readability, we use the term "connectivity strength"; however, in diffusion MRI, FA reflects diffusion properties rather than direct measures of connection efficacy or information transfer and should be interpreted accordingly (Figley et al., 2022).

For each modality, group comparisons were conducted using independent t-tests to assess differences between typically and atypically lateralised individuals, as well as lateralised versus non-lateralised groups. Effect sizes (Cohen's d) were computed to quantify the magnitude of these differences, with values of 0.2, 0.5, and 0.8 corresponding to small (~85% population overlap), medium (~67% overlap), and large (~53% overlap) effects, respectively (Cohen, 1977). P-values were corrected for multiple comparisons using the false discovery rate (FDR), and nodes showing significant effects were identified.

Structure-function coupling

Structure-function coupling was computed using the 64 regions defined by the SENSAAS atlas (Labache et al., 2019). For each node, coupling was defined as the Pearson correlation between the non-zero elements of its regional structural connectivity profile (measured using fractional anisotropy, FA) and its functional connectivity profile (measured using resting-state fMRI correlation coefficients) (Baum et al., 2020) (Figure 2). Regional connectivity profiles for each participant were represented as vectors of connectivity strength from a single network node to all other nodes, excluding diagonal elements (Zarkali et al., 2021). This approach yielded a single coupling value per node, reflecting the relationship between its structural and functional connectivity patterns. Fisher's Z-transformation was applied to the resulting correlation coefficients to normalise the data for statistical analysis.

To visualise global structure-function coupling, Z-transformed coupling scores were averaged across participants for each node and mapped onto the cortical brain surface. Group comparisons were conducted using the PALM (Permutation Analysis of Linear Models) toolbox in FSL (Winkler et al., 2014), testing two contrasts: (1) bilateral vs lateralised language representation and (2) typical vs atypical language lateralisation. False discovery rate correction (FDR, $p < 0.05$) was applied across the 64 regions defined by the SENSAAS atlas to control for multiple comparisons. Covariates of no interest, including sex, age, and handedness, were incorporated into the model. Group differences were assessed using 10,000 permutations.

Posthoc analyses

To further investigate the relationship between structural and functional connectivity in language lateralisation, we conducted post-hoc analyses focusing exclusively on edge-level coupling for connections involving significant regions. Specifically, we used MATLAB (version R2023a) to extract edge-level connectivity values from these regions to all other brain areas and quantified structure-function coupling by multiplying resting-state functional MRI (rsfMRI) connectivity values with diffusion MRI-based fractional anisotropy (FA) for each connection. As in our main analyses, negative functional connectivity values were thresholded at zero before multiplication, ensuring that only positive rsfMRI connectivity values were used in computing coupling metrics.

Results

Participant characteristics

Out of 285 healthy participants, 241 were typically lateralised (mean age 25.5 ± 6.17 years, 49% female), while 44 were atypically lateralised (mean age 27.0 ± 7.86 years, 46% female). In terms of bilateral versus lateralised grouping, 259 participants were lateralised (right- or left-hemisphere lateralised; mean age 25.6 ± 6.21 years, 50% female), and 26 had bilateral language representation (mean age 27.2 ± 8.63 years, 31% female). The overall mean age of participants was 25.7 years (SD ± 6.5), with no significant age differences observed between the typical and atypical groups or between the lateralised and bilateral groups (t-test, $p > 0.05$).

Female participants comprised 48% of the total sample ($n = 138$), with no significant differences in gender distribution across the lateralisation groups (chi-square, $p > 0.05$). Handedness was evenly distributed, with 48% of participants being right-handed and 52% left-handed. No significant differences in handedness were found between the bilateral and lateralised groups (t-test, $p = 0.232$). However, a significant difference in handedness was observed between the typical and atypical groups (t-test, $p = 0.002$), with the atypical group having significantly lower Edinburgh Handedness Inventory scores, indicating a higher likelihood of left-handedness.

Average connectivity strength

Following FDR correction for multiple comparisons, only the right supramarginal gyrus (SMG7_R) exhibited a significant association with language lateralisation. Higher FA connectivity strength in this region was observed in typically lateralised individuals (pFDR = 0.016, Cohen's d = 0.41, Supplementary Figure 1b). No other associations in the

FA or rsfMRI modalities remained significant after correction. Additionally, no significant differences were found between lateralised and non-lateralised individuals (Supplementary Figure 1a), and no other nodes showed significant associations in the comparison between typical and atypical lateralisation (Supplementary Figure 1b).

Structure-function coupling

Overall, the structure-function coupling values were relatively low across all regions (Fisher $z < 0.4$). Visual inspection of the global structure-function coupling data showed that coupling is highest in amygdala, and lowest in the temporal lobe, based on averaged Fisher z-transformed values (Figure 3). The amygdala (Fisher $z = 0.41$ on the right, 0.36 on the left) exhibited consistently high coupling values (note that the amygdala is not visible in the figure as it is an internal structure). Similarly, midline regions such as the posterior cingulate gyrus (Fisher $z = 0.35$ on the left, 0.31 on the right) also demonstrated higher coupling compared to the rest of the nodes. Within cortical regions, coupling was more pronounced in the frontal lobe, where the supplementary motor area (SMA 2, Fisher $z = 0.38$ on the left, 0.35 on the right) and the pars orbitalis (F3OI, Fisher $z = 0.37$ on the left, 0.26 on the right) exhibited high values. The temporal lobe showed variable coupling, with regions such as the superior temporal sulcus displaying bilateral coupling (STS_1, Fisher $z = 0.32$ on both sides), while other temporal areas exhibited comparatively lower values. Coupling appeared relatively symmetric across hemispheres, with bilateral representation in regions such as the amygdala, posterior cingulate gyrus, and superior temporal sulcus. Slightly higher Fisher z-values were observed in the left hemisphere for regions including the supplementary motor area and inferior frontal gyrus. It is important to note, however, that these observations are based on visual inspection of averaged Fisher z-values and do not reflect statistical significance.

In the typical versus atypical lateralisation contrast, higher coupling in the typical lateralisation group was observed in the left precentral sulcus (prec3_L) ($t = 3.69$, Cohen's $d = 0.89$, $p = 2 \times 10^{-4}$, pFDR = 0.0128), which survived FDR adjustment (Figure 4). Other regions with higher coupling in the typical group, but not surviving FDR adjustment included the right superior temporal sulcus (STS1_R) ($t = 2.05$, Cohen's $d = 0.5$, $p = 0.022$, pFDR = 0.3888), the left amygdala (AMYG_L) ($t = 1.98$, Cohen's $d = 0.48$, $p = 0.024$, pFDR = 0.3888), and the left putamen (PUT3_L) ($t = 2.02$, Cohen's $d = 0.49$, $p = 0.024$, pFDR = 0.3888) (Supplementary Figure 2). Higher coupling in the atypical lateralisation group was observed in the left anterior insula (INSa3_L) ($t = 3.14$, Cohen's $d = 0.76$, $p = 7 \times 10^{-4}$, pFDR = 0.0288) and the right middle temporal gyrus

(T2_3_R) ($t = 3.20$, Cohen's $d = 0.77$, $p = 9 \times 10^{-4}$, pFDR = 0.0288), both of which survived FDR adjustment. Additional regions with higher coupling in the atypical group that did not survive FDR adjustment included the left middle temporal gyrus (T2_3_L) ($t = 2.52$, Cohen's $d = 0.61$, $p = 0.0064$, q?FDR = 0.1365) and the right fusiform gyrus (FUS4_R) ($t = 2.05$, Cohen's $d = 0.5$, $p = 0.023$, pFDR = 0.2995).

In the non-lateralised versus lateralised analysis, higher coupling in people with bilateral language representation was observed in the left anterior insula (INSa3_L) ($t = 3.31$, Cohen's $d = 0.86$, $p = 6 \times 10^{-4}$, pFDR = 0.0128), which was the only region to survive FDR adjustment (Figure 5). Additional regions with higher coupling in the bilateral group, but not surviving FDR adjustment, included the right middle temporal gyrus (T2_3_R) ($t = 2.63$, Cohen's $d = 0.68$, $p = 0.0072$, pFDR= 0.2304), the left middle temporal gyrus (T2_3_L) ($t = 2.15$, Cohen's $d = 0.56$, $p = 0.018$, pFDR = 0.2832), and the left frontal sulcus (f2_2_L) ($t = 1.90$, Cohen's $d = 0.49$, $p = 0.031$, pFDR = 0.332) (Supplementary Figure 3). In contrast, regions with higher coupling in the lateralised group included the left precentral sulcus (prec3_L) ($t = 3.03$, Cohen's $d = 0.79$, $p = 8 \times 10^{-4}$, pFDR = 0.0512), though it did not survive FDR adjustment, as well as the left superior temporal sulcus (STS2_L) ($t = 2.48$, Cohen's $d = 0.65$, $p = 0.0081$, pFDR = 0.2592) and the right superior temporal sulcus (STS1_R) ($t = 1.85$, Cohen's $d = 0.48$, $p = 0.035$, pFDR = 0.7424).

Posthoc analyses

Post-hoc analyses examined structure-function coupling across all connections involving the significant regions: left INSa3, right T2_3, and left prec3. Significant group differences emerged only for connections involving the INSa3_L. Coupling between the left INSa3 and the left INSa2 was significantly higher in atypically lateralised individuals compared to typical individuals ($t = 4.12$, pFDR = 0.0064, Cohen's $d = 0.71$, $N = 283$) (Figure 6). In lateralised versus non-lateralised individuals, coupling between the INSa3_L and INSa2_L was also higher in the non-lateralised group ($t = 5.45$, pFDR = 0.00016, Cohen's $d = 1.14$, $N = 283$) (Figure 7). Additionally, a significant difference was observed in the coupling between the INSa3_L and the T2_4_R, with non-lateralised individuals exhibiting higher coupling in non-lateralised individuals ($t = 4.04$, pFDR = 0.0267, Cohen's $d = 1.24$, $N = 43$).

No other connections, including those involving T2_3_R or prec3_L, retained significance after multiple comparison correction.

Discussion

To our knowledge, this is the first study to specifically investigate SC-FC coupling concerning functional language lateralisation. By integrating rsfMRI and diffusion MRI modalities, we explored nodal connectivity strength and SC-FC coupling to uncover distinct patterns across language laterality groups. Consistent with our hypotheses, SC-FC coupling differentiated typical and atypical individuals. Unexpectedly, however, atypical individuals were not marked by reduced coupling, as hypothesised; instead, they exhibited heightened coupling in specific regions, including the left anterior insula and right middle temporal gyrus, while SC-FC couplingof the left precentral sulcus was associated with typical language dominance. Non-lateralised individuals showed increased coupling in the left anterior insula compared to lateralised groups, suggesting its role in supporting non-lateralised language networks. Analyses of rsfMRI and diffusion MRI FA connectivity independently revealed no significant group differences in rsfMRI, while FA connectivity strength in the right supramarginal gyrus was associated with typical language dominance.

SC-FC coupling – biological relevance

SC-FC coupling reflects the interplay between structural and functional connectivity, offering insights into how brain anatomy supports functional dynamics. Our findings reveal that SC-FC differentiates typical and atypical language lateralisation groups, with distinct patterns emerging in the left superior precentral sulcus, left anterior insula, and right MTG. High SC-FC coupling is associated with neural efficiency, where functional activity is tightly constrained by structural pathways, enabling energy-efficient and predictable communication (Haier et al., 1988; Neubauer & Fink, 2009). This efficiency stems from structural scaffolding, as strong coupling reinforces stable, anatomically grounded networks (Buckner & Krienen, 2013). For instance, the strong coupling in typical lateralisation likely reflects reliance on well-established language networks that support consistent hemispheric dominance for language tasks.

At a global level, overall coupling values were low, consistent with previous studies showing reduced coupling in higher-order regions (Figure 3; Buckner & Krienen, 2013; Chamberland et al., 2017; Vázquez-Rodríguez et al., 2019). This trend aligns with the atlas used, which focuses on supramodal regions involved in language sentence production (Labache et al., 2019). Lower SC-FC coupling in higher-order regions, such as those involved in language, reflects their greater cognitive flexibility and capacity for dynamic reconfiguration (Chamberland et al., 2017; Smith, 2016; Zimmermann et al., 2018). This flexibility reduces reliance on structural pathways, enabling adaptive functional networks for complex linguistic and cognitive tasks (Diamond, 2020).

In contrast, regions distinguishing laterality groups exhibited stronger coupling, reflecting signalling constraints essential for polysensory integration (Buckner & Krienen, 2013; Vázquez-Rodríguez et al., 2019). These regions likely achieve efficient language processing through stable SC-FC coupling, avoiding frequent reconfiguration or heavy neuromodulation (Suárez et al., 2020). This pattern aligns with the Neural Efficiency Hypothesis of Intelligence, which posits that individuals with higher cognitive abilities exhibit more efficient neural processing, requiring less activation during cognitive tasks (Haier et al., 1988; Popp et al., 2024; Wang, 2021). While our study did not study language performance differences between groups, heightened SC-FC coupling in higher-order regions, such as the inferior frontal lobe, has been linked to improved reading performance in other studies (Kotoski et al., 2024), suggesting a similar mechanism may support language proficiency.

Contrary to expectations, atypical individuals did not exhibit reduced SC-FC coupling. Variability in SC-FC coupling across regions and groups reinforces the idea that coupling is highly context-dependent and not uniformly distributed. For example, while typical individuals showed increased coupling in the left precentral sulcus, atypical individuals did not show a mirrored increase in the right precentral sulcus (Figure 4). This lack of mirroring suggests that atypical individuals do not simply replicate typical lateralisation patterns in the opposite hemisphere. Instead, they exhibit distinct SC-FC coupling organisation, supporting the idea that typical and atypical individuals represent two distinct populations with different structural and functional language organisation. The observed patterns align with the concept of the brain operating near criticality, where regions balance stability and adaptability to optimise processing efficiency (Park & Friston, 2013). This balance enables different lateralisation profiles to rely on distinct structural-functional configurations, underscoring the diversity in neural mechanisms underlying language dominance.

Topology of SC-FC coupling in relation to language lateralisation

Our study identified the SC-FC coupling in the upper part of the left precentral sulcus was associated with typical language lateralisation. The prominence of this region in our findings likely reflects its unique developmental, structural, and functional characteristics. Emerging around the 24th week of gestation and running approximately parallel to the central sulcus (Chi et al., 1977), the precentral sulcus (PrCS) provides early anatomical scaffolding essential for articulatory and phonological processing (Matchin & Hickok, 2020). The morphology of PrCS demonstrates a consistent left-hemispheric bias, defined by a higher incidence of its presence in the left hemisphere

compared to the right, across both humans and non-human primates (Juch et al., 2005; S. S. Keller et al., 2007; Ono et al., 1990). Deeper left PrCS morphology has been linked to right-handedness (Amunts et al., 1996; Foundas et al., 1998; Klöppel et al., 2007; Willems & Hagoort, 2009), which, in turn, correlates with left-hemisphere language dominance (Johnstone et al., 2021; Knecht et al., 2000). Keller et al. (2007, 2009) further demonstrated that sulci neighbouring the inferior frontal gyrus (IFG) (such as the PrCS and diagonal sulcus) contribute to leftward asymmetry in the IFG by increasing intrasulcal area, potentially facilitating leftward language lateralisation (Powell et al., 2012). Given that our findings specifically pertain to SC-FC coupling in the upper PrCS, caution is warranted in directly applying broader conclusions from whole-PrCS morphology. Further studies incorporating detailed morphological analyses of PrCS subdivisions could clarify its precise contribution to language lateralisation.

The anterior insula was a key region where heightened SC-FC coupling differentiated atypical from typical language lateralisation, as well as non-lateralised individuals from lateralised ones. This finding was not replicated in separate analyses of rsfMRI or diffusion MRI FA connectivity, highlighting the unique value of SC-FC coupling in capturing the integrated dynamics of structural and functional networks underlying language lateralisation. While leftward structural asymmetry of the anterior insula has been linked to typical language dominance (Biduła & Króliczak, 2015; S. S. Keller et al., 2011), atypical individuals often show reduced or reversed asymmetry (Greve et al., 2013). In our study, however, heightened SC-FC coupling in the left anterior insula was associated with atypical lateralisation, raising questions about its left-lateralised focus. Network-based studies have previously shown associations between FA connectivity in both the left and right anterior insula and strongly atypical lateralisation (Andrulyte, Zago, et al., 2025), though these findings reflect a different scope—FA connectivity rather than SC-FC coupling. Conceptualised as a "code translator," the anterior insula is thought to bridge structural and functional networks, enabling efficient communication between neural systems that support linguistic and non-linguistic processes, including attention and salience detection (Cai & Van Der Haegen, 2015; Molnar-Szakacs & Uddin, 2022; Uddin, 2015). In people with atypical and non-lateralised language representation, heightened coupling may indicate a supportive mechanism that allows for enhanced cross-hemispheric communication while remaining structurally anchored within left-lateralised pathways. This integrative role may explain why the anterior insula remains persistently involved in atypical and non-lateralised individuals, functioning as an adaptive mediator of language networks that supports the dynamic coordination of structural and functional asymmetries.

A key distinction emerged between right-lateralised and bilateral individuals in how SC-FC coupling was organised within the anterior insula. In atypical individuals (including right-lateralised and non-lateralised), SC-FC coupling was primarily driven by intrahemispheric connectivity within the left anterior insula-specifically, between INSa_3 and INSa_2 (Figure 6). In non-lateralised as compared to lateralised individuals, an additional coupling effect was observed in the interhemispheric connectivity between the left INSa_3 and the right middle temporal gyrus (MTG; T2_4) (Figure 7). This suggests that while both right-lateralised and bilateral individuals rely on intrahemispheric insular connectivity within the left hemisphere, supported by structural scaffolding (Biduła & Króliczak, 2015), non-lateralised individuals additionally recruit interhemispheric connections involving the MTG. The functional significance of this additional connectivity remains unclear, but its selective presence in these individuals suggests it may reflect an alternative strategy for language network organisation in non-lateralised individuals. Further research is needed to determine whether this connectivity pattern has functional consequences or represents variability in SC-FC coupling across individuals.

Interestingly, while our results indicated increased SC-FC coupling in the right MTG (T2_3) in atypically lateralised individuals, post-hoc analyses did not identify significant edge-level coupling differences between groups. This raises questions regarding the precise role of right MTG connectivity in atypical lateralisation. Previous studies have demonstrated that increased FA nodal degree in the right MTG is associated with right hemisphere language dominance (Zahnert et al., 2023) and semantic performance in patients with left temporal lobe epilepsy (Audrain et al., 2018). These findings suggest that the right MTG may act as a compensatory structure for linguistic functions in the absence of typical leftward dominance. While only the right MTG survived multiple comparisons in our analysis, the left MTG also showed a trend toward significance (pFDR = 0.1365, Cohen's d = 0.5; Supplementary Figure 2), suggesting that both hemispheres may contribute to language processing in atypically lateralised individuals. This aligns with previous network-based diffusion MRI studies, which have demonstrated that individuals with atypical language dominance exhibit increased connectivity between the MTG and other temporal regions, both inter- and intra-hemispherically (Andrulyte, Zago, et al., 2025).

Methodological considerations

The methodological framework of this study reflects both its strengths and areas requiring further exploration. One of the key methodological considerations was focusing exclusively on positive rsfMRI correlations for SC-FC coupling, prioritising clearer interpretability of results. Although negative correlations between nodes in rsfMRI

studies are documented, especially in higher-order regions (Fox et al., 2005; Uddin et al., 2009), their biological significance remains debated (J. B. Keller et al., 2015; Murphy et al., 2009; Nir et al., 2020; Weissenbacher et al., 2009). Although this choice may limit the scope of interpretation, focusing on positive correlations aligns with the majority of SC-FC coupling studies and supports robust and interpretable analyses (Baum et al., 2020).

Interpreting the structural connectivity underlying SC-FC coupling also presents methodological challenges, particularly in relation to FA. While FA is widely employed in diffusion MRI studies, it does not directly reflect white matter integrity but rather serves as a proxy for microstructural organisation (Jones et al., 2013; Rheault et al., 2020). Its sensitivity to fibre architecture, particularly in regions with multiple crossing fibres, can obscure meaningful biological interpretations (Jeurissen et al., 2013). In association and commissural pathways, where multiple fibre populations intersect, the diffusion tensor model is unable to resolve distinct orientations, leading to artificially reduced FA values even when connectivity remains intact (Tournier et al., 2011). As a result, variations in FA between groups may arise from diverse sources-including differences in fibre complexity, neuroinflammatory processes, or acquisition-related artefacts-rather than reflecting true differences in connectivity (Figley et al., 2022). To mitigate these limitations, future studies should consider integrating more advanced diffusion models that refine white matter characterisation (Daducci et al., 2015; Mayer et al., 2022; H. Zhang et al., 2012).

Another important limitation relates to the diffusion MRI FA connectivity matrices, where 70-95% of connections were missing for key nodes, including the left anterior insula, left precentral sulcus, and right MTG. This highlights that SC-FC coupling in these regions may reflect only a subset of connections rather than a comprehensive view of node connectivity. Additionally, the use of a group atlas assumes uniform functional boundaries across individuals, which may fail to account for significant interindividual variability, particularly in transmodal cortices where functional boundaries are known to differ (Gordon et al., 2017). This potential misalignment could affect the accuracy of SC-FC coupling measurements, leading to certain regions being underrepresented or overemphasised in the analysis (Suárez et al., 2020).

Future research should address these limitations by investigating interindividual variability through participant-specific parcellations to better capture the functional organisation of higher-order regions. Examining the connections to and from specific regions, such as the anterior insula, MTG, and precentral sulcus, will be critical for understanding their roles in hemispheric language dominance. Additionally, studies should

employ a range of language tasks and alternative atlases to provide a more comprehensive understanding of the functional and structural dynamics underlying SC-FC coupling. These steps are vital to advancing our understanding of SC-FC coupling's role in language lateralisation and delineating the specific contributions of key cortical regions.

Conclusion

Our findings establish SC-FC coupling as a valuable approach for distinguishing typical and atypical language lateralisation and lateralised and non-lateralised profiles. The left anterior insula emerged as a key region, supporting left-hemisphere access in atypical and non-lateralised individuals, while the right MTG was uniquely linked to atypical lateralisation, potentially aiding cross-hemispheric processing. Typical language dominance was linked to stronger coupling in the left superior precentral sulcus, reaffirming its critical role in hemispheric asymmetry. These results emphasise the importance of these regions in language lateralisation and invite further exploration into their specific contributions.

Funding

Ieva Andrulyte - BBSRC DTP training grant BB/T008695/1
Space for other authors (if applicable)

CREDIT authorship contribution statement

Ieva Andrulyte - conceptualisation, data analysis, funding acquisition, writing - original draft
Space for other authors

References:

Amunts, K., Schlaug, G., Schleicher, A., Steinmetz, H., Dabringhaus, A., Roland, P. E., & Zilles, K. (1996). Asymmetry in the Human Motor Cortex and Handedness. *NeuroImage*, *4*(3), 216–222. https://doi.org/10.1006/nimg.1996.0073

Andrulyte, I., De Bezenac, C., Branzi, F., Forkel, S. J., Taylor, P. N., & Keller, S. S. (2024). The Relationship between White Matter Architecture and Language Lateralization in the Healthy Brain. *The Journal of Neuroscience: The Official*

Journal of the Society for Neuroscience, *44*(50), e0166242024. https://doi.org/10.1523/JNEUROSCI.0166-24.2024

Andrulyte, I., Demirkan, E., Branzi, F. M., Bonnett, L. J., & Keller, S. S. (2025). *Does white matter structure relate to hemispheric language lateralisation? A systematic review*. https://doi.org/10.1101/2025.01.04.631320

Andrulyte, I., Zago, L., Jobard, G., Lemaitre, H., Rheault, F., Keller, S. S., & Petit, L. (2025). *Distinct Structural Connectivity Patterns Associated with Variations in Language Lateralisation*. https://doi.org/10.1101/2025.02.04.636415

Audrain, S., Barnett, A. J., & McAndrews, M. P. (2018). Language network measures at rest indicate individual differences in naming decline after anterior temporal lobe resection. *Human Brain Mapping*, *39*(11), 4404–4419. https://doi.org/10.1002/hbm.24281

Avants, B., Tustison, N. J., & Song, G. (2009). Advanced Normalization Tools: V1.0. *The Insight Journal*. https://doi.org/10.54294/uvnhin

Avena-Koenigsberger, A., Misic, B., & Sporns, O. (2018). Communication dynamics in complex brain networks. *Nature Reviews Neuroscience*, *19*(1), 17–33. https://doi.org/10.1038/nrn.2017.149

Basser, P. J., Mattiello, J., & LeBihan, D. (1994). MR diffusion tensor spectroscopy and imaging. *Biophysical Journal*, *66*(1), 259–267. https://doi.org/10.1016/S0006-3495(94)80775-1

Baum, G. L., Cui, Z., Roalf, D. R., Ciric, R., Betzel, R. F., Larsen, B., Cieslak, M., Cook, P. A., Xia, C. H., Moore, T. M., Ruparel, K., Oathes, D. J., Alexander-Bloch, A. F., Shinohara, R. T., Raznahan, A., Gur, R. E., Gur, R. C., Bassett, D. S., & Satterthwaite, T. D. (2020). Development of structure–function coupling in human brain networks during youth. *Proceedings of the National*

Academy of Sciences, *117*(1), 771–778. https://doi.org/10.1073/pnas.1912034117

Betzel, R. (2020, October 4). *Network neuroscience and the connectomics revolution*. arXiv.Org. https://arxiv.org/abs/2010.01591v1

Biduła, S. P., & Króliczak, G. (2015). Structural asymmetry of the insula is linked to the lateralization of gesture and language. *European Journal of Neuroscience*, *41*(11), 1438–1447. https://doi.org/10.1111/ejn.12888

Biswal, B., Zerrin Yetkin, F., Haughton, V. M., & Hyde, J. S. (1995). Functional connectivity in the motor cortex of resting human brain using echo-planar mri. *Magnetic Resonance in Medicine*, *34*(4), 537–541. https://doi.org/10.1002/mrm.1910340409

Buckner, R. L., & Krienen, F. M. (2013). The evolution of distributed association networks in the human brain. *Trends in Cognitive Sciences*, *17*(12), 648–665. https://doi.org/10.1016/j.tics.2013.09.017

Cai, Q., & Van Der Haegen, L. (2015). What can atypical language hemispheric specialization tell us about cognitive functions? *Neuroscience Bulletin*, *31*(2), 220–226. https://doi.org/10.1007/s12264-014-1505-5

Chamberland, M., Girard, G., Bernier, M., Fortin, D., Descoteaux, M., & Whittingstall, K. (2017). On the Origin of Individual Functional Connectivity Variability: The Role of White Matter Architecture. *Brain Connectivity*, *7*(8), 491–503. https://doi.org/10.1089/brain.2017.0539

Chang, Y.-H. A., Kemmotsu, N., Leyden, K. M., Kucukboyaci, N. E., Iragui, V. J., Tecoma, E. S., Kansal, L., Norman, M. A., Compton, R., Ehrlich, T. J., Uttarwar, V. S., Reyes, A., Paul, B. M., & McDonald, C. R. (2017). Multimodal imaging of language reorganization in patients with left temporal lobe

epilepsy. *Brain and Language*, *170*, 82–92. https://doi.org/10.1016/j.bandl.2017.03.012

Chi, J. G., Dooling, E. C., & Gilles, F. H. (1977). Gyral development of the human brain. *Annals of Neurology*, *1*(1), 86–93. https://doi.org/10.1002/ana.410010109

Cohen, J. (1977). *Statistical Power Analysis for the Behavioral Sciences*. Elsevier. https://doi.org/10.1016/C2013-0-10517-X

Daducci, A., Dal Palu, A., Lemkaddem, A., & Thiran, J.-P. (2015). COMMIT: Convex Optimization Modeling for Microstructure Informed Tractography. *IEEE Transactions on Medical Imaging*, *34*(1), 246–257. https://doi.org/10.1109/TMI.2014.2352414

Descoteaux, M., Deriche, R., Knosche, T. R., & Anwander, A. (2009). Deterministic and Probabilistic Tractography Based on Complex Fibre Orientation Distributions. *IEEE Transactions on Medical Imaging*, *28*(2), 269–286. https://doi.org/10.1109/TMI.2008.2004424

Diamond, A. (2020). Executive functions. In *Handbook of Clinical Neurology* (Vol. 173, pp. 225–240). Elsevier. https://doi.org/10.1016/B978-0-444-64150-2.00020-4

Figley, C. R., Uddin, M. N., Wong, K., Kornelsen, J., Puig, J., & Figley, T. D. (2022). Potential Pitfalls of Using Fractional Anisotropy, Axial Diffusivity, and Radial Diffusivity as Biomarkers of Cerebral White Matter Microstructure. *Frontiers in Neuroscience*, *15*, 799576. https://doi.org/10.3389/fnins.2021.799576

Fornito, A., & Bullmore, E. T. (2015). Reconciling abnormalities of brain network structure and function in schizophrenia. *Current Opinion in Neurobiology*, *30*, 44–50. https://doi.org/10.1016/j.conb.2014.08.006

Foundas, A. L., Eure, K. F., Luevano, L. F., & Weinberger, D. R. (1998). MRI asymmetries of Broca's area: The pars triangularis and pars opercularis. *Brain and Language*, *64*(3), 282–296. https://doi.org/10.1006/brln.1998.1974

Fox, M. D., Snyder, A. Z., Vincent, J. L., Corbetta, M., Van Essen, D. C., & Raichle, M. E. (2005). The human brain is intrinsically organized into dynamic, anticorrelated functional networks. *Proceedings of the National Academy of Sciences*, *102*(27), 9673–9678. https://doi.org/10.1073/pnas.0504136102

Girard, G., Whittingstall, K., Deriche, R., & Descoteaux, M. (2014). Towards quantitative connectivity analysis: Reducing tractography biases. *NeuroImage*, *98*, 266–278. https://doi.org/10.1016/j.neuroimage.2014.04.074

Gordon, E. M., Laumann, T. O., Gilmore, A. W., Newbold, D. J., Greene, D. J., Berg, J. J., Ortega, M., Hoyt-Drazen, C., Gratton, C., Sun, H., Hampton, J. M., Coalson, R. S., Nguyen, A. L., McDermott, K. B., Shimony, J. S., Snyder, A. Z., Schlaggar, B. L., Petersen, S. E., Nelson, S. M., & Dosenbach, N. U. F. (2017). Precision Functional Mapping of Individual Human Brains. *Neuron*, *95*(4), 791-807.e7. https://doi.org/10.1016/j.neuron.2017.07.011

Greve, D. N., Van Der Haegen, L., Cai, Q., Stufflebeam, S., Sabuncu, M. R., Fischl, B., & Brysbaert, M. (2013). A Surface-based Analysis of Language Lateralization and Cortical Asymmetry. *Journal of Cognitive Neuroscience*, *25*(9), 1477–1492. https://doi.org/10.1162/jocn_a_00405

Hagmann, P., Cammoun, L., Gigandet, X., Meuli, R., Honey, C. J., Wedeen, V. J., & Sporns, O. (2008). Mapping the Structural Core of Human Cerebral Cortex. *PLOS Biology*, *6*(7), e159. https://doi.org/10.1371/journal.pbio.0060159

Haier, R. J., Siegel, B. V., Nuechterlein, K. H., Hazlett, E., Wu, J. C., Paek, J., Browning, H. L., & Buchsbaum, M. S. (1988). Cortical glucose metabolic rate

correlates of abstract reasoning and attention studied with positron emission tomography. *Intelligence*, *12*(2), 199–217. https://doi.org/10.1016/0160-2896(88)90016-5

Hebb, D. O. (1949). *The organization of behavior.* Wiley.

Huntenburg, J. M., Bazin, P.-L., Goulas, A., Tardif, C. L., Villringer, A., & Margulies, D. S. (2017). A Systematic Relationship Between Functional Connectivity and Intracortical Myelin in the Human Cerebral Cortex. *Cerebral Cortex*, *27*(2), 981–997. https://doi.org/10.1093/cercor/bhx030

Ibrahim, G. M., Morgan, B. R., Doesburg, S. M., Taylor, M. J., Pang, E. W., Donner, E., Go, C. Y., Rutka, J. T., & Snead, O. C. (2015). Atypical language laterality is associated with large-scale disruption of network integration in children with intractable focal epilepsy. *Cortex*, *65*, 83–88. https://doi.org/10.1016/j.cortex.2014.12.016

Jeurissen, B., Leemans, A., Tournier, J.-D., Jones, D. K., & Sijbers, J. (2013). Investigating the prevalence of complex fiber configurations in white matter tissue with diffusion magnetic resonance imaging. *Human Brain Mapping*, *34*(11), 2747–2766. https://doi.org/10.1002/hbm.22099

Johnstone, L. T., Karlsson, E. M., & Carey, D. P. (2021). Left-Handers Are Less Lateralized Than Right-Handers for Both Left and Right Hemispheric Functions. *Cerebral Cortex*, bhab048. https://doi.org/10.1093/cercor/bhab048

Joliot, M., Jobard, G., Naveau, M., Delcroix, N., Petit, L., Zago, L., Crivello, F., Mellet, E., Mazoyer, B., & Tzourio-Mazoyer, N. (2015). AICHA: An atlas of intrinsic connectivity of homotopic areas. *Journal of Neuroscience Methods*, *254*, 46–59. https://doi.org/10.1016/j.jneumeth.2015.07.013

Joliot, M., Tzourio-Mazoyer, N., & Mazoyer, B. (2016). Intra-hemispheric intrinsic connectivity asymmetry and its relationships with handedness and language Lateralization. *Neuropsychologia*, *93*(Pt B), 437–447. https://doi.org/10.1016/j.neuropsychologia.2016.03.013

Jones, D. K., Knösche, T. R., & Turner, R. (2013). White matter integrity, fiber count, and other fallacies: The do's and don'ts of diffusion MRI. *NeuroImage*, *73*, 239–254. https://doi.org/10.1016/j.neuroimage.2012.06.081

Juch, H., Zimine, I., Seghier, M. L., Lazeyras, F., & Fasel, J. H. D. (2005). Anatomical variability of the lateral frontal lobe surface: Implication for intersubject variability in language neuroimaging. *NeuroImage*, *24*(2), 504–514. https://doi.org/10.1016/j.neuroimage.2004.08.037

Keller, J. B., Hedden, T., Thompson, T. W., Anteraper, S. A., Gabrieli, J. D. E., & Whitfield-Gabrieli, S. (2015). Resting-state anticorrelations between medial and lateral prefrontal cortex: Association with working memory, aging, and individual differences. *Cortex*, *64*, 271–280. https://doi.org/10.1016/j.cortex.2014.12.001

Keller, S. S., Highley, J. R., Garcia-Finana, M., Sluming, V., Rezaie, R., & Roberts, N. (2007). Sulcal variability, stereological measurement and asymmetry of Broca's area on MR images. *Journal of Anatomy*, *211*(4), 534–555. https://doi.org/10.1111/j.1469-7580.2007.00793.x

Keller, S. S., Roberts, N., García-Fiñana, M., Mohammadi, S., Ringelstein, E. B., Knecht, S., & Deppe, M. (2011). *Can the Language-dominant Hemisphere Be Predicted by Brain Anatomy?*

Keller, S. S., Roberts, N., & Hopkins, W. (2009). A comparative magnetic resonance imaging study of the anatomy, variability, and asymmetry of Broca's area in

the human and chimpanzee brain. *Journal of Neuroscience*, *29*(46), 14607–14616. https://doi.org/10.1523/JNEUROSCI.2892-09.2009

Klöppel, S., Van Eimeren, T., Glauche, V., Vongerichten, A., Münchau, A., Frackowiak, R. S. J., Büchel, C., Weiller, C., & Siebner, H. R. (2007). The effect of handedness on cortical motor activation during simple bilateral movements. *NeuroImage*, *34*(1), 274–280. https://doi.org/10.1016/j.neuroimage.2006.08.038

Knecht, S., Dräger, B., Deppe, M., Bobe, L., Lohmann, H., Flöel, A., Ringelstein, E.-B., & Henningsen, H. (2000). Handedness and hemispheric language dominance in healthy humans. *Brain*, *123*(12), 2512–2518. https://doi.org/10.1093/brain/123.12.2512

Kotoski, A., Liu, J., Morris, R., & Calhoun, V. (2024). Inter-Modality Source Coupling: A Fully-Automated Whole-Brain Data-Driven Structure-Function Fingerprint Shows Replicable Links to Reading in a Large-Scale (N~8K) Analysis. *IEEE Transactions on Biomedical Engineering*, *71*(12), 3383–3389. https://doi.org/10.1109/TBME.2024.3423703

Labache, L., Joliot, M., Saracco, J., Jobard, G., Hesling, I., Zago, L., Mellet, E., Petit, L., Crivello, F., Mazoyer, B., & Tzourio-Mazoyer, N. (2019). A SENtence Supramodal Areas AtlaS (SENSAAS) based on multiple task-induced activation mapping and graph analysis of intrinsic connectivity in 144 healthy right-handers. *Brain Structure and Function*, *224*(2), 859–882. https://doi.org/10.1007/s00429-018-1810-2

Labache, L., Mazoyer, B., Joliot, M., Crivello, F., Hesling, I., & Tzourio-Mazoyer, N. (2020). Typical and atypical language brain organization based on intrinsic

connectivity and multitask functional asymmetries. *eLife*, *9*, e58722. https://doi.org/10.7554/eLife.58722

Langs, G., Wang, D., Golland, P., Mueller, S., Pan, R., Sabuncu, M. R., Sun, W., Li, K., & Liu, H. (2016). Identifying Shared Brain Networks in Individuals by Decoupling Functional and Anatomical Variability. *Cerebral Cortex (New York, N.Y.: 1991)*, *26*(10), 4004–4014. https://doi.org/10.1093/cercor/bhv189

Lebel, C., Treit, S., & Beaulieu, C. (2019). A review of diffusion MRI of typical white matter development from early childhood to young adulthood. *NMR in Biomedicine*, *32*(4), e3778. https://doi.org/10.1002/nbm.3778

Legarreta, J. H., Petit, L., Rheault, F., Theaud, G., Lemaire, C., Descoteaux, M., & Jodoin, P.-M. (2021). Filtering in tractography using autoencoders (FINTA). *Medical Image Analysis*, *72*, 102126. https://doi.org/10.1016/j.media.2021.102126

Luppi, A. I., & Stamatakis, E. A. (2021). Combining network topology and information theory to construct representative brain networks. *Network Neuroscience*, *5*(1), 96–124. https://doi.org/10.1162/netn_a_00170

Maier-Hein, K. H., Neher, P. F., Houde, J.-C., Côté, M.-A., Garyfallidis, E., Zhong, J., Chamberland, M., Yeh, F.-C., Lin, Y.-C., Ji, Q., Reddick, W. E., Glass, J. O., Chen, D. Q., Feng, Y., Gao, C., Wu, Y., Ma, J., He, R., Li, Q., … Descoteaux, M. (2017). The challenge of mapping the human connectome based on diffusion tractography. *Nature Communications*, *8*(1), 1349. https://doi.org/10.1038/s41467-017-01285-x

Margulies, D. S., Ghosh, S. S., Goulas, A., Falkiewicz, M., Huntenburg, J. M., Langs, G., Bezgin, G., Eickhoff, S. B., Castellanos, F. X., Petrides, M., Jefferies, E., & Smallwood, J. (2016). Situating the default-mode network along a principal

gradient of macroscale cortical organization. *Proceedings of the National Academy of Sciences*, *113*(44), 12574–12579. https://doi.org/10.1073/pnas.1608282113

Matchin, W., & Hickok, G. (2020). The Cortical Organization of Syntax. *Cerebral Cortex*, *30*(3), 1481–1498. https://doi.org/10.1093/cercor/bhz180

Mayer, C., Nägele, F. L., Petersen, M., Frey, B. M., Hanning, U., Pasternak, O., Petersen, E., Gerloff, C., Thomalla, G., & Cheng, B. (2022). Free-water diffusion MRI detects structural alterations surrounding white matter hyperintensities in the early stage of cerebral small vessel disease. *Journal of Cerebral Blood Flow & Metabolism*, *42*(9), 1707–1718. https://doi.org/10.1177/0271678X221093579

Mazoyer, B., Mellet, E., Perchey, G., Zago, L., Crivello, F., Jobard, G., Delcroix, N., Vigneau, M., Leroux, G., Petit, L., Joliot, M., & Tzourio-Mazoyer, N. (2016). BIL&GIN: A neuroimaging, cognitive, behavioral, and genetic database for the study of human brain lateralization. *NeuroImage*, *124*, 1225–1231. https://doi.org/10.1016/j.neuroimage.2015.02.071

Mazoyer, B., Zago, L., Jobard, G., Crivello, F., Joliot, M., Perchey, G., Mellet, E., Petit, L., & Tzourio-Mazoyer, N. (2014). Gaussian Mixture Modeling of Hemispheric Lateralization for Language in a Large Sample of Healthy Individuals Balanced for Handedness. *PLOS ONE*, *9*(6), e101165. https://doi.org/10.1371/journal.pone.0101165

Medaglia, J. D., Huang, W., Karuza, E. A., Kelkar, A., Thompson-Schill, S. L., Ribeiro, A., & Bassett, D. S. (2017). Functional alignment with anatomical networks is associated with cognitive flexibility. *Nature Human Behaviour*, *2*(2), 156–164. https://doi.org/10.1038/s41562-017-0260-9

Molnar-Szakacs, I., & Uddin, L. Q. (2022). Anterior insula as a gatekeeper of executive control. *Neuroscience & Biobehavioral Reviews*, *139*, 104736. https://doi.org/10.1016/j.neubiorev.2022.104736

Murphy, K., Birn, R. M., Handwerker, D. A., Jones, T. B., & Bandettini, P. A. (2009). The impact of global signal regression on resting state correlations: Are anti-correlated networks introduced? *NeuroImage*, *44*(3), 893–905. https://doi.org/10.1016/j.neuroimage.2008.09.036

Neubauer, A. C., & Fink, A. (2009). Intelligence and neural efficiency. *Neuroscience & Biobehavioral Reviews*, *33*(7), 1004–1023. https://doi.org/10.1016/j.neubiorev.2009.04.001

Nir, T., Jacob, Y., Huang, K.-H., Schwartz, A. E., Brallier, J. W., Ahn, H., Kundu, P., Tang, C. Y., Delman, B. N., McCormick, P. J., Sano, M., Deiner, S., Baxter, M. G., & Mincer, J. S. (2020). Resting-state functional connectivity in early postanaesthesia recovery is characterised by globally reduced anticorrelations. *British Journal of Anaesthesia*, *125*(4), 529–538. https://doi.org/10.1016/j.bja.2020.06.058

Ono, M., Kubik, S., & Abernathey, C. D. (1990). *Atlas of the cerebral sulci*. G. Thieme Verlag□; Thieme Medical Publishers.

Park, H.-J., & Friston, K. (2013). Structural and Functional Brain Networks: From Connections to Cognition. *Science*, *342*(6158), 1238411. https://doi.org/10.1126/science.1238411

Petit, L., Ali, K. M., Rheault, F., Boré, A., Cremona, S., Corsini, F., De Benedictis, A., Descoteaux, M., & Sarubbo, S. (2023). The structural connectivity of the human angular gyrus as revealed by microdissection and diffusion

tractography. *Brain Structure and Function*, *228*(1), 103–120. https://doi.org/10.1007/s00429-022-02551-5

Popp, J. L., Thiele, J. A., Faskowitz, J., Seguin, C., Sporns, O., & Hilger, K. (2024). Structural-functional brain network coupling predicts human cognitive ability. *NeuroImage*, *290*, 120563. https://doi.org/10.1016/j.neuroimage.2024.120563

Powell, J. L., Kemp, G. J., Roberts, N., & García-Finaña, M. (2012). Sulcal morphology and volume of Broca's area linked to handedness and sex. *Brain and Language*, *121*(3), 206–218. https://doi.org/10.1016/j.bandl.2012.03.003

Preti, M. G., & Van De Ville, D. (2019). Decoupling of brain function from structure reveals regional behavioral specialization in humans. *Nature Communications*, *10*(1), 4747. https://doi.org/10.1038/s41467-019-12765-7

Rheault, F., Poulin, P., Valcourt Caron, A., St-Onge, E., & Descoteaux, M. (2020). Common misconceptions, hidden biases and modern challenges of dMRI tractography. *Journal of Neural Engineering*, *17*(1), 011001. https://doi.org/10.1088/1741-2552/ab6aad

Rolls, E. T., Deco, G., Huang, C.-C., & Feng, J. (2022). The human language effective connectome. *NeuroImage*, *258*, 119352. https://doi.org/10.1016/j.neuroimage.2022.119352

Sarwar, T., Tian, Y., Yeo, B. T. T., Ramamohanarao, K., & Zalesky, A. (2021). Structure-function coupling in the human connectome: A machine learning approach. *NeuroImage*, *226*, 117609. https://doi.org/10.1016/j.neuroimage.2020.117609

Shi, J., Kirihara, K., Tada, M., Fujioka, M., Usui, K., Koshiyama, D., Araki, T., Chen, L., Kasai, K., & Aihara, K. (2021). Criticality in the Healthy Brain. *Frontiers in Network Physiology*, *1*, 755685. https://doi.org/10.3389/fnetp.2021.755685

Skudlarski, P., Jagannathan, K., Calhoun, V. D., Hampson, M., Skudlarska, B. A., & Pearlson, G. (2008). Measuring brain connectivity: Diffusion tensor imaging validates resting state temporal correlations. *NeuroImage*, *43*(3), 554–561. https://doi.org/10.1016/j.neuroimage.2008.07.063

Smith, S. (2016). Linking cognition to brain connectivity. *Nature Neuroscience*, *19*(1), 7–9. https://doi.org/10.1038/nn.4206

Sotiropoulos, S. N., & Zalesky, A. (2019). Building connectomes using diffusion MRI: Why, how and but. *NMR in Biomedicine*, *32*(4), e3752. https://doi.org/10.1002/nbm.3752

Straathof, M., Sinke, M. R., Dijkhuizen, R. M., & Otte, W. M. (2019). A systematic review on the quantitative relationship between structural and functional network connectivity strength in mammalian brains. *Journal of Cerebral Blood Flow & Metabolism*, *39*(2), 189–209. https://doi.org/10.1177/0271678X18809547

Suárez, L. E., Markello, R. D., Betzel, R. F., & Misic, B. (2020). Linking Structure and Function in Macroscale Brain Networks. *Trends in Cognitive Sciences*, *24*(4), 302–315. https://doi.org/10.1016/j.tics.2020.01.008

Tao, Y., Liu, B., Zhang, X., Li, J., Qin, W., Yu, C., & Jiang, T. (2015). The Structural Connectivity Pattern of the Default Mode Network and Its Association with Memory and Anxiety. *Frontiers in Neuroanatomy*, *9*. https://doi.org/10.3389/fnana.2015.00152

Tournier, J., Mori, S., & Leemans, A. (2011). Diffusion tensor imaging and beyond. *Magnetic Resonance in Medicine*, *65*(6), 1532–1556. https://doi.org/10.1002/mrm.22924

Turner, R., Le Bihan, D., Maier, J., Vavrek, R., Hedges, L. K., & Pekar, J. (1990). Echo-planar imaging of intravoxel incoherent motion. *Radiology*, *177*(2), 407–414. https://doi.org/10.1148/radiology.177.2.2217777

Uddin, L. Q. (2015). Salience processing and insular cortical function and dysfunction. *Nature Reviews Neuroscience*, *16*(1), 55–61. https://doi.org/10.1038/nrn3857

Uddin, L. Q., Clare Kelly, A. M., Biswal, B. B., Xavier Castellanos, F., & Milham, M. P. (2009). Functional connectivity of default mode network components: Correlation, anticorrelation, and causality. *Human Brain Mapping*, *30*(2), 625–637. https://doi.org/10.1002/hbm.20531

Vázquez-Rodríguez, B., Suárez, L. E., Markello, R. D., Shafiei, G., Paquola, C., Hagmann, P., van den Heuvel, M. P., Bernhardt, B. C., Spreng, R. N., & Misic, B. (2019). Gradients of structure–function tethering across neocortex. *Proceedings of the National Academy of Sciences of the United States of America*, *116*(42), 21219–21227. https://doi.org/10.1073/pnas.1903403116

Wang, Z. (2021). The neurocognitive correlates of brain entropy estimated by resting state fMRI. *NeuroImage*, *232*, 117893. https://doi.org/10.1016/j.neuroimage.2021.117893

Weissenbacher, A., Kasess, C., Gerstl, F., Lanzenberger, R., Moser, E., & Windischberger, C. (2009). Correlations and anticorrelations in resting-state functional connectivity MRI: A quantitative comparison of preprocessing strategies. *NeuroImage*, *47*(4), 1408–1416. https://doi.org/10.1016/j.neuroimage.2009.05.005

Wilke, M., & Schmithorst, V. J. (2006). A combined bootstrap/histogram analysis approach for computing a lateralization index from neuroimaging data.

NeuroImage, *33*(2), 522–530. https://doi.org/10.1016/j.neuroimage.2006.07.010

Willems, R. M., & Hagoort, P. (2009). Hand preference influences neural correlates of action observation. *Brain Research*, *1269*, 90–104. https://doi.org/10.1016/j.brainres.2009.02.057

Winkler, A. M., Ridgway, G. R., Webster, M. A., Smith, S. M., & Nichols, T. E. (2014). Permutation inference for the general linear model. *NeuroImage*, *92*(100), 381–397. https://doi.org/10.1016/j.neuroimage.2014.01.060

Wu, D., Fan, L., Song, M., Wang, H., Chu, C., Yu, S., & Jiang, T. (2020). Hierarchy of Connectivity–Function Relationship of the Human Cortex Revealed through Predicting Activity across Functional Domains. *Cerebral Cortex*, *30*(8), 4607–4616. https://doi.org/10.1093/cercor/bhaa063

Yeo, B. T. T., Krienen, F. M., Eickhoff, S. B., Yaakub, S. N., Fox, P. T., Buckner, R. L., Asplund, C. L., & Chee, M. W. L. (2016). Functional Specialization and Flexibility in Human Association Cortex. *Cerebral Cortex*, *26*(1), 465–465. https://doi.org/10.1093/cercor/bhv260

Zahnert, F., Kräling, G., Melms, L., Belke, M., Kleinholdermann, U., Timmermann, L., Hirsch, M., Jansen, A., Mross, P., Menzler, K., Habermehl, L., & Knake, S. (2023). Diffusion magnetic resonance imaging connectome features are predictive of functional lateralization of semantic processing in the anterior temporal lobes. *Human Brain Mapping*, *44*(2), 496–508. https://doi.org/10.1002/hbm.26074

Zarkali, A., McColgan, P., Leyland, L.-A., Lees, A. J., Rees, G., & Weil, R. S. (2021). Organisational and neuromodulatory underpinnings of structural-functional

connectivity decoupling in patients with Parkinson's disease. *Communications Biology*, *4*(1), 1–13. https://doi.org/10.1038/s42003-020-01622-9

Zhang, F., Daducci, A., He, Y., Schiavi, S., Seguin, C., Smith, R. E., Yeh, C.-H., Zhao, T., & O'Donnell, L. J. (2022). Quantitative mapping of the brain's structural connectivity using diffusion MRI tractography: A review. *NeuroImage*, *249*, 118870. https://doi.org/10.1016/j.neuroimage.2021.118870

Zhang, H., Schneider, T., Wheeler-Kingshott, C. A., & Alexander, D. C. (2012). NODDI: Practical in vivo neurite orientation dispersion and density imaging of the human brain. *NeuroImage*, *61*(4), 1000–1016. https://doi.org/10.1016/j.neuroimage.2012.03.072

Zhang, Z., Liao, W., Chen, H., Mantini, D., Ding, J.-R., Xu, Q., Wang, Z., Yuan, C., Chen, G., Jiao, Q., & Lu, G. (2011). Altered functional–structural coupling of large-scale brain networks in idiopathic generalized epilepsy. *Brain*, *134*(10), 2912–2928. https://doi.org/10.1093/brain/awr223

Zimmermann, J., Griffiths, J. D., & McIntosh, A. R. (2018). Unique Mapping of Structural and Functional Connectivity on Cognition. *The Journal of Neuroscience*, *38*(45), 9658–9667. https://doi.org/10.1523/JNEUROSCI.0900-18.2018

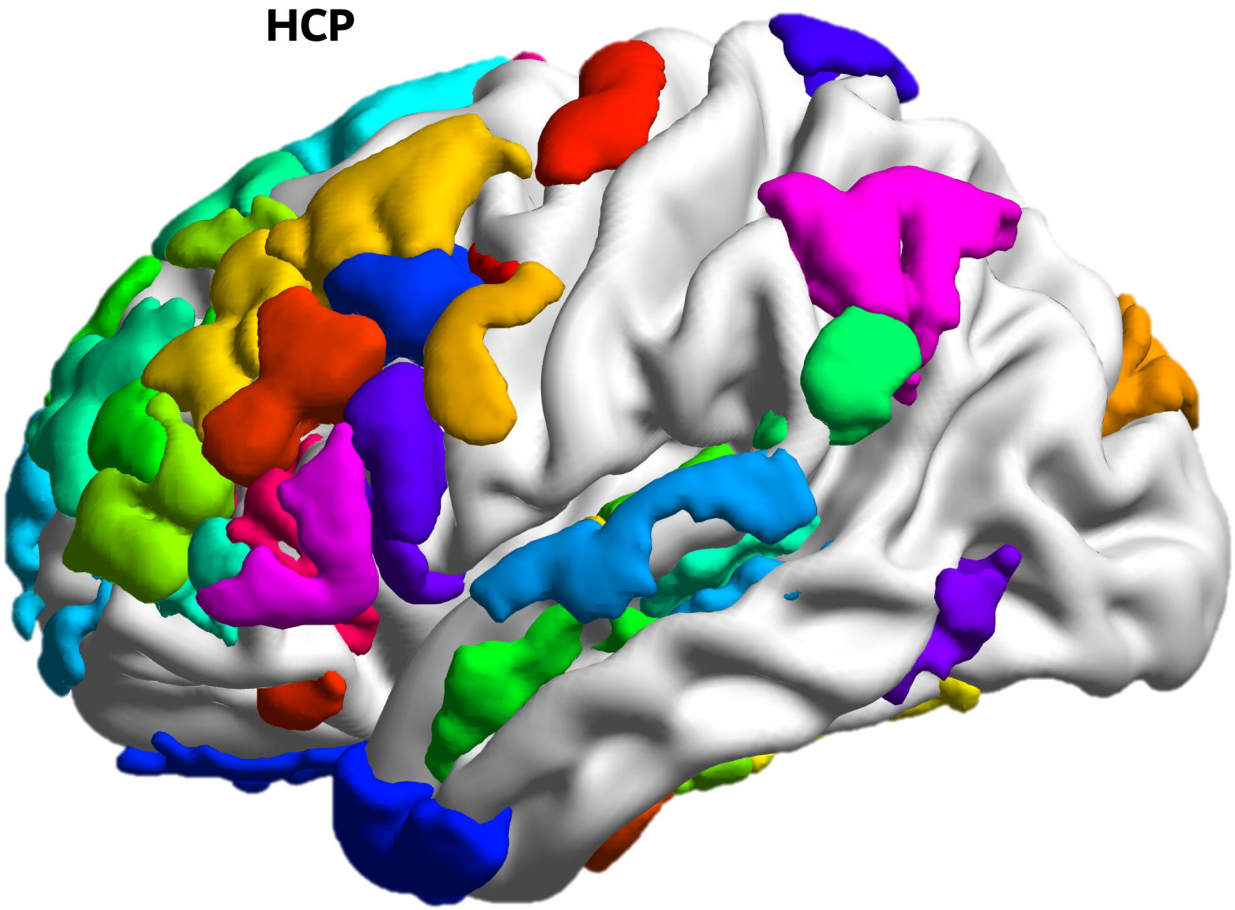
HCP

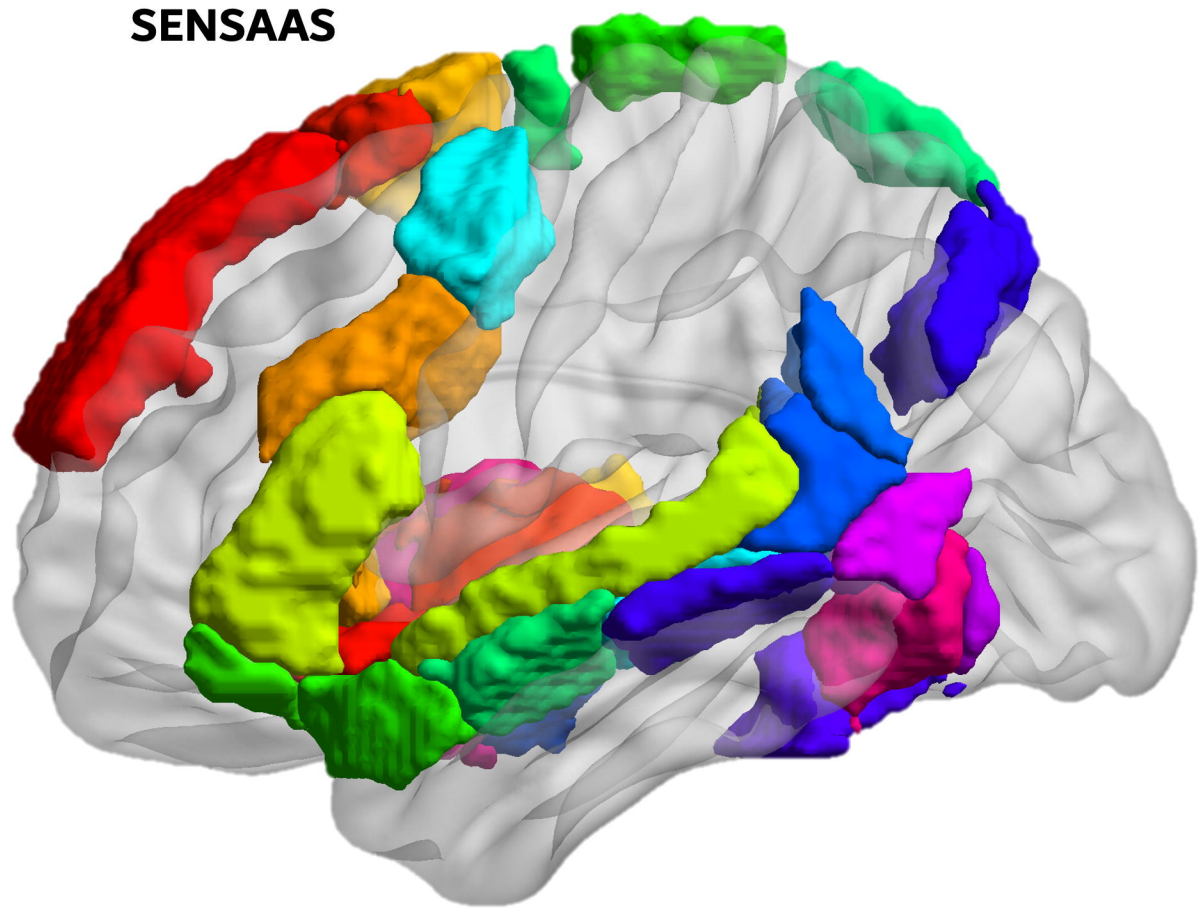
SENSAAS

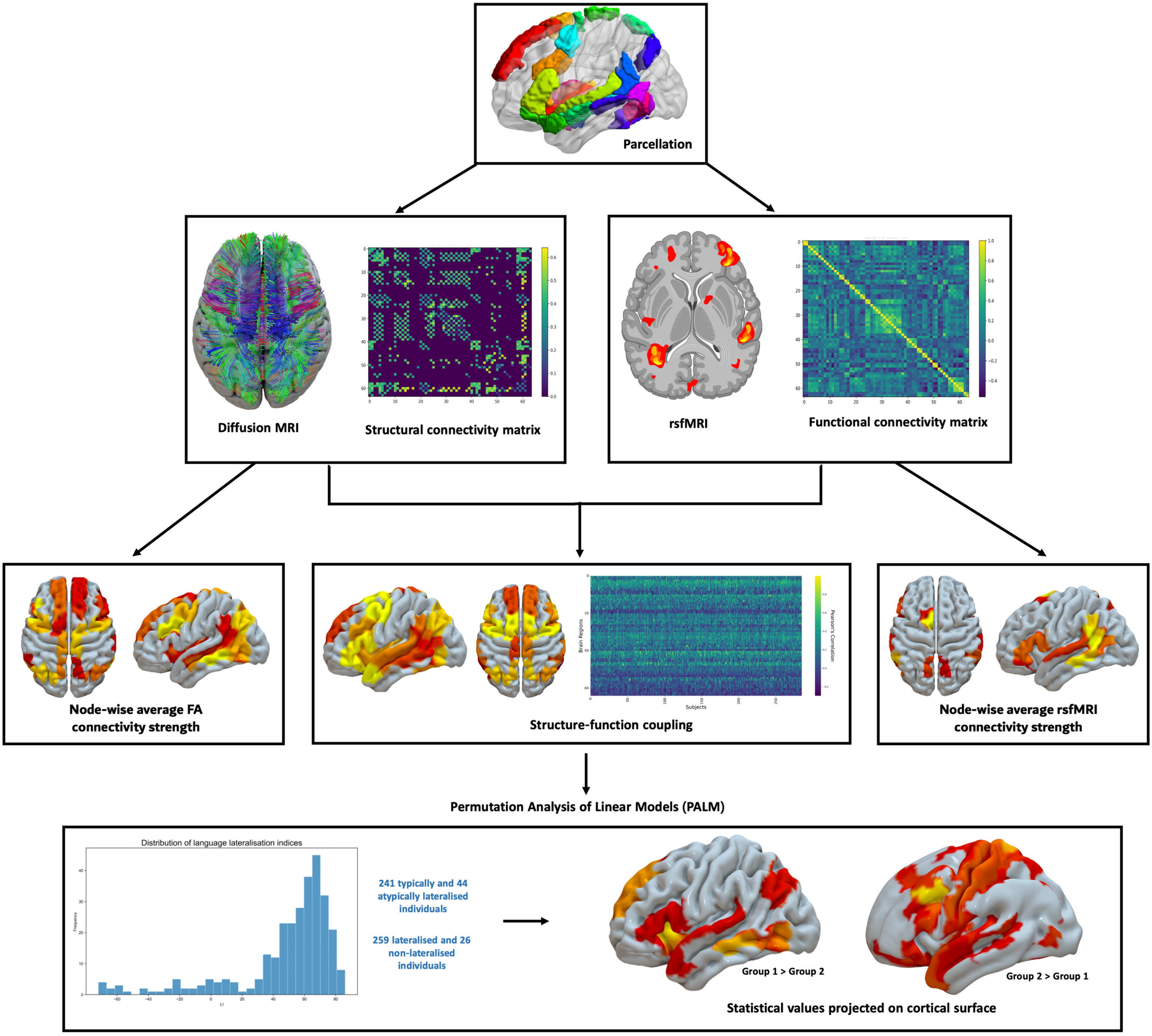
Parcellation
Diffusion MRI
Structural connectivity matrix
rsfMRI
Functional connectivity matrix
Node-wise average FA connectivity strength
Brain Regions
Subjects
Pearson's Correlation
Structure-function coupling
Node-wise average rsfMRI connectivity strength
Permutation Analysis of Linear Models (PALM)
Distribution of language lateralisation indices
Frequency
LI
241 typically and 44 atypically lateralised individuals
259 lateralised and 26 non-lateralised individuals
Group 1 > Group 2
Group 2 > Group 1
Statistical values projected on cortical surface

Global structure-function coupling

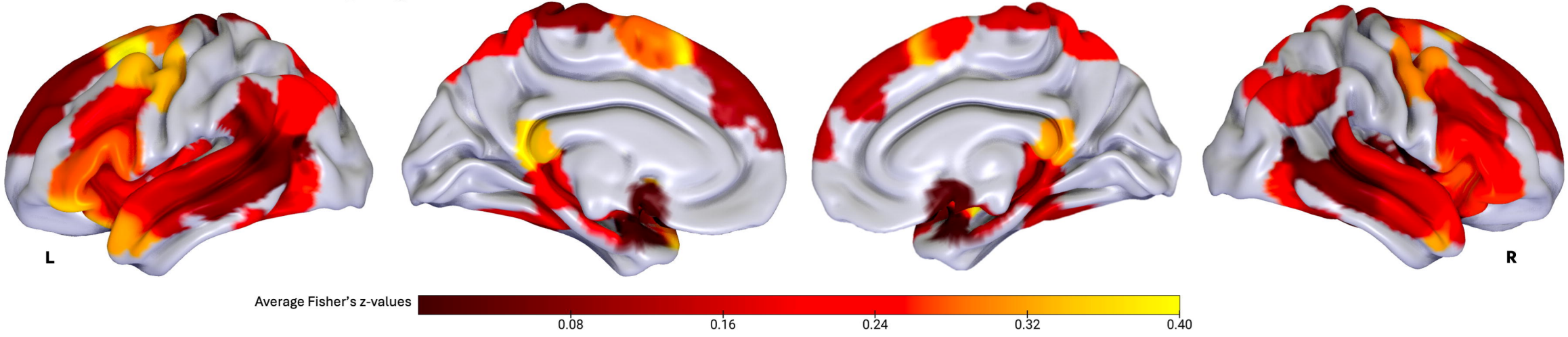

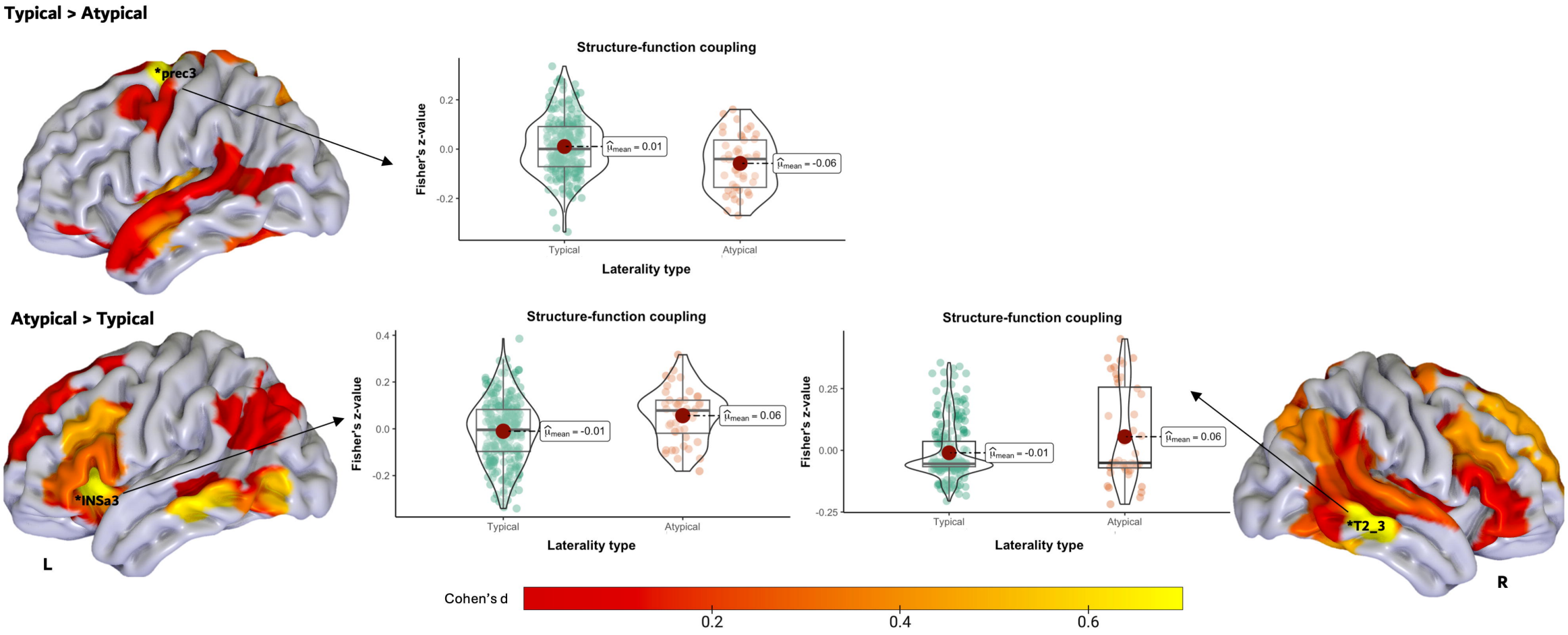
Typical > Atypical
*prec3
Structure-function coupling
Fisher's z-value
0.2
0.0
-0.2
$\hat{\mu}_{mean}$ = 0.01
$\hat{\mu}_{mean}$ = -0.06
Typical
Atypical
Laterality type
Atypical > Typical
*INSa3
L
Structure-function coupling
Fisher's z-value
0.4
0.2
0.0
-0.2
$\hat{\mu}_{mean}$ = -0.01
$\hat{\mu}_{mean}$ = 0.06
Typical
Atypical
Laterality type
Structure-function coupling
Fisher's z-value
0.25
0.00
-0.25
$\hat{\mu}_{mean}$ = -0.01
$\hat{\mu}_{mean}$ = 0.06
Typical
Atypical
Laterality type
*T2_3
R
Cohen's d
0.2
0.4
0.6

Nonlateralised > Lateralised

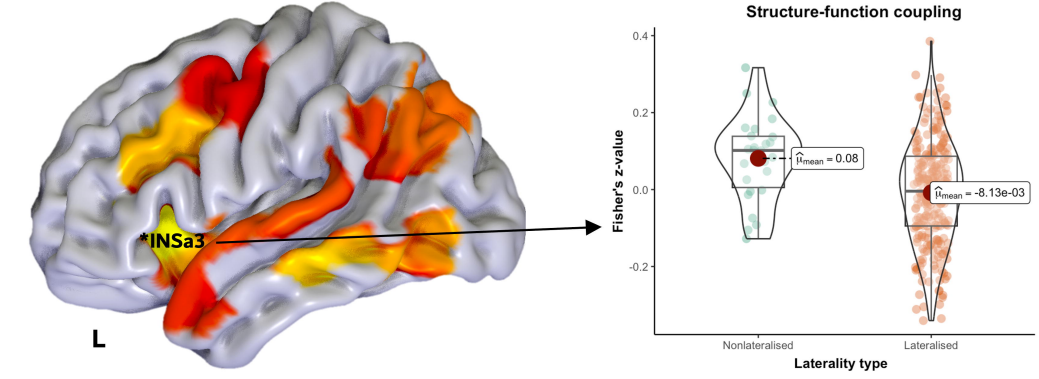

Cohen's d

0.2 0.4 0.6

Atypical > Typical

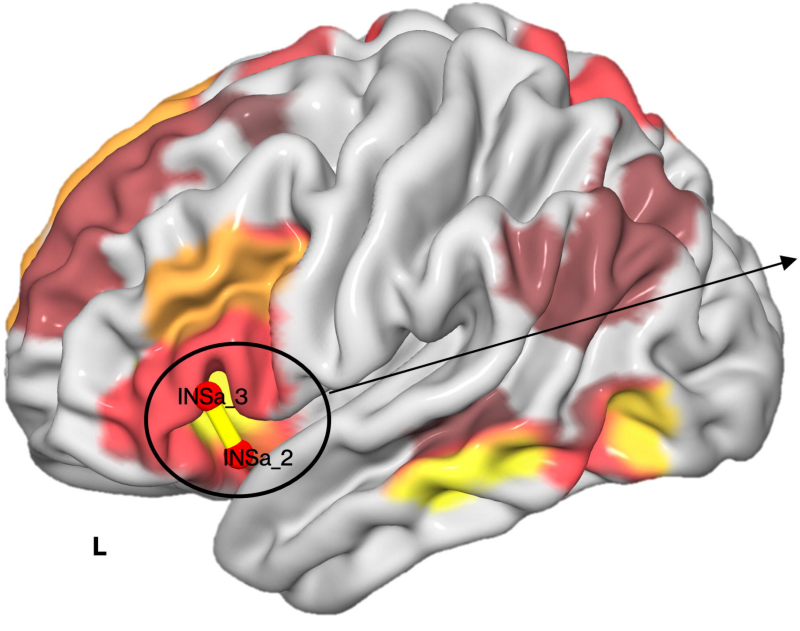

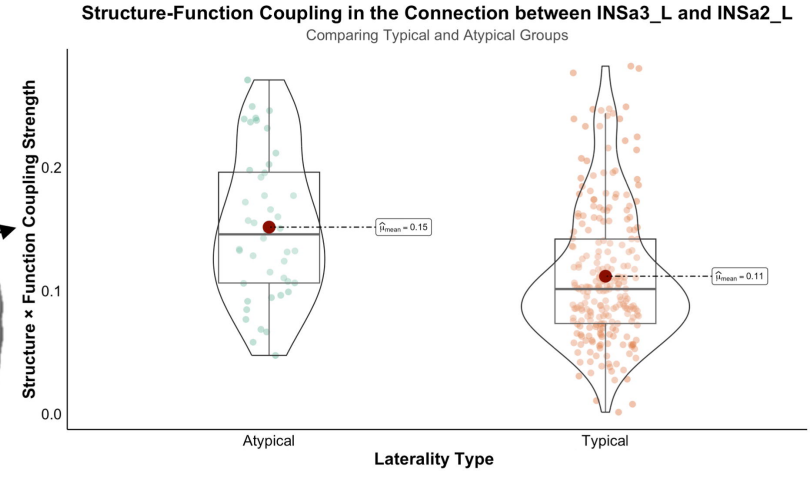

Nonlateralised > Lateralised

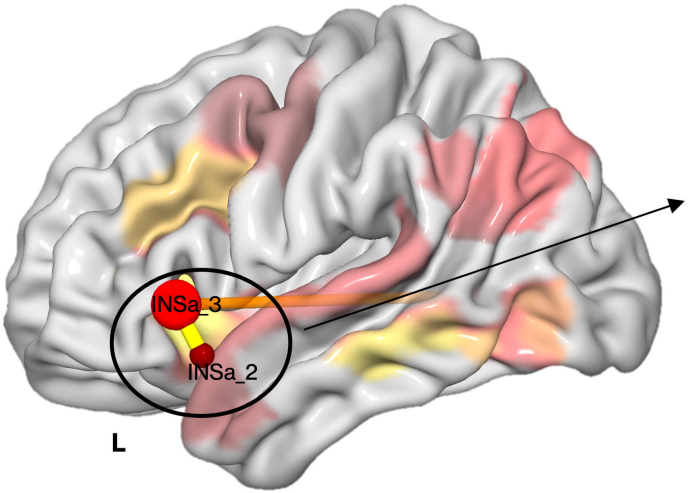

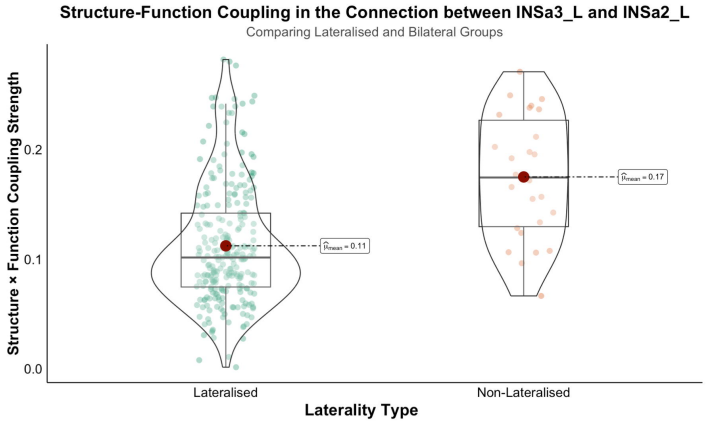

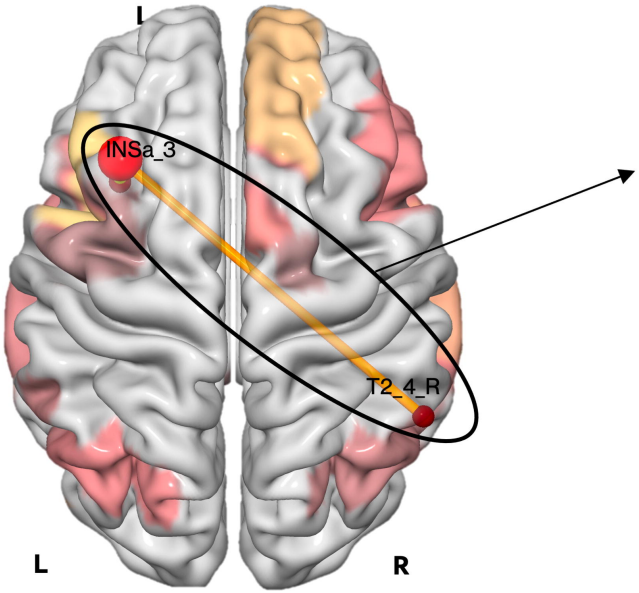

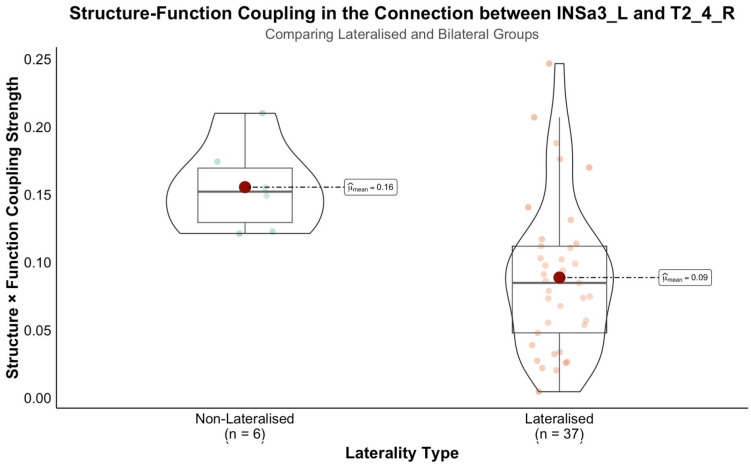

Figure 1. **Brain regions included in the analysis.** Laterality indices (LIs) were calculated across the whole brain using the AICHA atlas (Joliot et al., 2015). The SENSAAS atlas, developed for the BIL&GIN dataset, was then used to define regions of interest implicated in sentence production (Labache et al., 2019).

Figure 2. **Pipeline for computing structure-function coupling.** This figure illustrates the methodological steps for assessing structure-function coupling within the brain. The brain is first divided into distinct regions of interest (nodes) using a predefined atlas. Diffusion MRI data is processed to generate a structural connectivity matrix. This matrix quantifies the strength of white matter connections between each pair of nodes, using fractional anisotropy (FA) as a measure of connectivity. Resting-state fMRI (rsfMRI) data is used to create a functional connectivity matrix, representing the temporal correlations in neuronal activity between each pair of nodes, calculated using Pearson's correlation. For each node, average FA connectivity strength is computed as the mean FA value of its structural connections, and average rsfMRI connectivity strength is computed as the mean functional connectivity value of its connections. Structure-function coupling is computed by correlating corresponding entries in the structural and functional connectivity matrices using Pearson's correlation, yielding a coupling measure for each node. This results in a measure of structure-function coupling for each region. Finally, differences in structure-function coupling between groups are statistically assessed using permutation analysis for linear models (PALM) implemented in FSL with 10,000 permutations. This analysis identifies regions where the relationship between structural and functional connectivity differs significantly between the groups.

Figure 3. **Global structure-function coupling, quantified by average Fisher's z-values across all participants.** The colour map represents the strength of coupling across brain regions, with yellow indicating areas of higher coupling and dark red indicating areas of lower coupling. The lateral, medial, and dorsal views provide a comprehensive visualisation of the spatial distribution of structure-function coupling averaged across the entire cohort.

Figure 4. **Significant group differences in structure–function coupling between individuals with atypical and typical language lateralisation.** This figure presents cortical projections of regions where structure–function coupling significantly differed between individuals with atypical (LI < 18) and typical (LI > 18) language lateralisation for language production. Statistical comparisons were conducted using a t-test within the FSL PALM framework with 10,000 permutations. The colour scale represents Cohen's d effect sizes, with red indicating smaller effect sizes and yellow indicating larger effect sizes. Regions that survived FDR correction ($p_{FDR} < 0.05$) are marked with an asterisk (*), highlighting areas where structure–function coupling was either greater in atypical compared to typical individuals or vice versa. Violin plots illustrate the magnitude and direction of effects, showing how coupling strengths differ between groups in regions where atypical lateralisation is associated with either increased or decreased coupling relative to the typical group. Anatomical labels indicate key regions, including the anterior insula (INSa3), upper part of precentral sulcus (prec3), and middle temporal gyrus (T2_3), where significant differences were observed.

Figure 5. **Significant group differences in structure–function coupling between individuals with lateralised and non-lateralised language representation.** This figure presents cortical projections of regions where structure–function coupling significantly differed between individuals with lateralised (LI > |20 |) and non-lateralised (20 ≤ LI ≤ 20) language representation for language production. Statistical comparisons were conducted using a t-test within the FSL PALM framework with 10,000 permutations. The colour scale represents Cohen's d effect sizes, with red indicating smaller effect sizes and yellow indicating larger effect sizes. Regions that survived FDR correction (pFDR < 0.05) are marked with an asterisk (*), highlighting areas where structure–function coupling was significantly greater in non-lateralised compared to lateralised individuals. Violin plots display the distribution of structure–function coupling values for the significant region, with non-corrected p-values reported for visualisation purposes. Anatomical label: INSa3 – anterior insula 3.

Figure 6. **Post-hoc analyses of edge-level structure–function coupling differences between individuals with atypical and typical language lateralisation.** This figure presents the connection where post-hoc analyses identified significant group differences in structure–function coupling between atypically (LI < 18) and typically (LI > 18) lateralised individuals. The colours projected on the cortical surface, represents Cohen's *d* effect sizes as shown in Figure 4. Post-hoc analyses revealed a significant difference in the connection between the left INSa3 and the left INSa2, with atypically lateralised individuals exhibiting significantly higher coupling compared to typically lateralised individuals (t = 4.12, pFDR = 0.0064, Cohen's d = 0.71, N = 283).

Figure 7. **Post-hoc analyses of edge-level structure–function coupling differences between individuals with non-lateralised and lateralised language representation.** This figure presents connections where post-hoc analyses identified significant group differences in structure–function coupling between non-lateralised (-20≤ LI ≤ 20) and lateralised (LI > |20|) individuals. The colours projected on the cortical surface represent Cohen's d effect sizes, as shown in Figure 5, while the colour bar represents t-values for edge-level coupling strength. Non-lateralised individuals exhibited significantly higher coupling between the left INSa3 and the left INSa2 (t = 5.45, pFDR = 0.00016, Cohen's d = 1.14, N = 283) and between the left INSa3 and the right T2_4 (t = 4.04, pFDR = 0.0267, Cohen's d = 1.24, N = 43). Violin plots display the distribution of structure–function coupling values for these connections.

Supplementary Figure 1. **Group-averaged connectivity strength for FA and rsfMRI data, visualised using Cohen's d.** This figure examines connectivity related to language production, specifically comparing groups based on their degree of language lateralisation. Panel (a) compares individuals with lateralised language representation (left- or right-hemisphere dominance for language) to those with non-lateralised (or bilateral) language representation. Panel (b) compares individuals with typical left-hemisphere lateralisation for language to those with atypical lateralisation (either right-hemisphere dominance or bilateral representation). Blue regions indicate greater connectivity strength in the non-lateralised group compared to the lateralised group (a) or in the atypically lateralised group compared to the typically lateralised group (b). Conversely, red regions indicate greater connectivity strength in the lateralised group compared to the non-lateralised group (a) or in the typically

lateralised group compared to the atypically lateralised group (b). Only in the comparison between typically and atypically lateralised groups (panel b) did a region survive FDR correction (pFDR < 0.05): *SMG7 - supramarginal gyrus 7, which showed greater connectivity in the typically lateralised group.

Supplementary Figure 2. **Whole-brain differences in structure–function coupling between typical and atypical language lateralisation groups.** This figure presents whole-brain projections of structure–function coupling differences between individuals with typical (LI > 18) and atypical (LI < 18) language lateralisation. Results were obtained using a t-test within the FSL PALM framework with 10,000 permutations. The colour scale represents Cohen's d effect sizes. Regions that survived FDR correction (pFDR < 0.05) are marked with an asterisk (*), as shown in Figure 4.

Supplementary Figure 3. **Whole-brain differences in structure–function coupling between individuals with lateralised and bilateral language representation.** This figure presents whole-brain projections of structure–function coupling differences between individuals with lateralised (LI > |20 |, encompassing both left (LI > 20) and right (LI < 20) lateralisation) and bilateral (20≤ LI ≤ 20) language representation during language production. Statistical comparisons were conducted using a t-test within the FSL PALM framework with 10,000 permutations. The colour scale represents Cohen's d effect sizes, with red indicating smaller effect sizes and yellow indicating larger effect sizes. Regions that survived FDR correction (pFDR < 0.05) are marked with an asterisk (*).